Catalysis Today 284 (2017) 129–136

Contents lists available at ScienceDirect

Catalysis Today

journal homepage: www.elsevier.com/locate/cattod

Peroxo group enhanced nanorutile as visible light active photocatalyst

Tamás Gyulavári[a,b], Zsolt Pap[a,c,d,e], Gábor Kovács[a,b,c,d], Lucian Baia[c,d], Milica Todea[d], Klára Hernádi[a,b], Gábor Veréb[a,f,*]

[a] Research Group of Environmental Chemistry, Institute of Chemistry, University of Szeged, H-6720, Szeged, Tisza Lajos krt. 103, Hungary
[b] Department of Applied and Environmental Chemistry, University of Szeged, H-6720, Szeged, Rerrich tér 1, Hungary
[c] Faculty of Physics, Babes-Bolyai University, RO-400084, Cluj-Napoca, M. Kogalniceanu 1, Romania
[d] Institute for Interdisciplinary Research on Bio-Nano-Sciences, Babes-Bolyai University, RO-400271, Cluj-Napoca, Treboniu Laurian 42, Romania
[e] Institute of Environmental Science and Technology, University of Szeged, H-6720, Szeged, Tisza Lajos krt. 103, Hungary
[f] Department of Process Engineering, Faculty of Engineering, University of Szeged, H-6725, Szeged, Moszkvai krt. 9, Hungary

ARTICLE INFO

Article history:
Received 15 July 2016
Received in revised form
29 September 2016
Accepted 6 November 2016
Available online 18 November 2016

Keywords:
Titanium dioxide
Rutile
Peroxo group
Phenol
Visible light excitability

ABSTRACT

Hydrogen peroxide was applied during the synthesis to enhance the visible light excitability of nanosized (<10 nm), pure rutile phase titanium dioxides synthesized by a facile, sol-gel method at low temperature. Different amounts of hydrogen peroxide were used during the synthesis to form peroxo groups on the surface of TiO_2-s. As-prepared photocatalysts were characterized by X-ray diffraction (XRD), diffuse reflectance spectroscopy (DRS), infrared spectroscopy (IR), and X-ray photoelectron spectroscopy (XPS). The photocatalytic activity of the catalysts were investigated by phenol, Rhodamine B dye and coumarin degradation under visible light irradiation. Evonik Aeroxide P25 TiO_2 and commercial rutile phase titanium dioxide were used as reference photocatalysts. First order derivative of DRS spectra showed enhanced visible light excitability in the case of $Ti:H_2O_2 = 1:2$ ratio (applied during the synthesis). XPS measurements confirmed the formation of peroxo groups in this specific TiO_2. Photocatalytic measurements pointed out that this TiO_2 had by far the best photocatalytic performance, exceeding the photocatalytic activity of Aeroxide P25 and commercial rutile as well. This activity gain was attributed to the presence of peroxo groups on the surface.

1. Introduction

Heterogeneous photocatalysis is one of the most promising advanced oxidation process and it is extensively investigated since the discovery of water splitting using titanium dioxide (TiO_2) [1]. TiO_2 based photocatalysis have been widely studied for water treatment applications due to its ability to decompose various kinds of organic pollutants even toxic, chemically stable and persistent contaminants like phenol [2–7], organic dyes [8,9], pesticides [8,10], pharmaceuticals [11,12], moreover, this method has high potential in disinfection [2,6,7,13–15] processes. It is imperative to develop visible light active photocatalysts for indoor applications (e.g. air-cleaning and self-cleaning surfaces) in order to utilize artificial light due to the negligible amount of UV photons under usual internal lighting conditions. Extending TiO_2 light absorption into the visible light region can also be beneficial for outdoor applications in case of natural solar irradiation (~45% of the solar spectrum is in the visible range).

There are many different approaches in the literature to prepare visible-light active TiO_2-s, like doping with various elements (e.g. nitrogen, iron, iodine, silver, gold, sulfur) [4–7,9,16,17], sensitizing with dyes [18,19], deposition of noble metals [12,20] or by preparing composites [20,21]. The photocatalytic efficiency can be increased by enhancing the visible light absorption of TiO_2 via the adsorption of hydrogen peroxide on the surface thus forming yellow-colored Ti-peroxo species [22,23]. A relatively novel approach to enhance the visible light activity of TiO_2 is to anchor Ti-peroxo groups on the surface using hydrogen-peroxide (H_2O_2) during the synthesis procedure, which increases the visible light absorption [18,24–27] thus amplifying the efficiency. Amorphous [25], anatase [18] or mixed phase [24,26,27] TiO_2-s were investigated, however forming peroxo groups on the surface of pure nanosized rutile in order to increase the visible light sensitivity have not been reported to our best knowledge, even though rutile has generally higher visible light activity [28,29] than anatase phase.

* Corresponding author at: Research Group of Environmental Chemistry, Institute of Chemistry, University of Szeged, H-6720, Szeged, Tisza Lajos krt. 103, Hungary.
E-mail address: verebg@mk.u-szeged.hu (G. Veréb).

http://dx.doi.org/10.1016/j.cattod.2016.11.012
0920-5861/

Based on the above-mentioned literature, in this study a facile, cost-effective synthesis method is presented to obtain nanosized (<10 nm) pure rutile phase TiO_2 containing peroxo groups with enhanced visible light sensitivity without the requirement of costly calcination.

2. Experimental

2.1. Materials

For the synthesis of rutile photocatalysts, titanium(IV) butoxide (Sigma-Aldrich, reagent grade, 97%), hydrochloric acid (VWR Chemicals; 37%), hydrogen peroxide (Sigma-Aldrich; 30%) and ultrapure water (Millipore Milli-Q) were used.

The photocatalytic efficiencies were determined using phenol (Spektrum 3D; analytical grade), Rhodamine B dye (Reanal; ≥99.9%) as model water contaminant, and the formation of hydroxyl radicals were followed by the degradation of coumarin (Sigma Aldrich; ≥99%).

The reference photocatalysts were commercially available Evonik Aeroxide P25, and rutile-phase titanium dioxide produced by US Research Nanomaterials Inc. (named as US-R.N. Rutile).

2.2. Synthesis

In our previous publication [30] nanosized rutile was obtained using Ti(IV) butoxide ($Ti(O\text{-}nBu)_4$) as precursor. To obtain pure rutile, H^+ concentration has to be set to a specific value, since both higher and lower acid concentration can lead to the formation of anatase. The optimal amount of reactants was the following: $Ti(O\text{-}nBu)_4$: HCl: H_2O = 1:3:50. In the present study different amounts of hydrogen-peroxide were also added applying the following molar ratios: $Ti(O\text{-}nBu)_4$: H_2O_2: HCl: H_2O = 1:1–4:3:50 to form peroxo groups on the surface of TiO_2 (these samples were named as Rutile-H1-H4 according to the used molar ratio of H_2O_2 compared to Ti ions). 7.83 mL hydrochloric acid and 3.22–12.88 mL hydrogen-peroxide was added in 19.84–12.46 mL Milli-Q water during intensive magnetic stirring, then 10.64 mL $Ti(O\text{-}nBu)_4$ was added dropwise (1 mL min^{-1}) to the solution. Ice bath was applied to prevent the decomposition of H_2O_2 caused by the exothermic hydrolysis procedure. The addition of $Ti(O\text{-}nBu)_4$ to the solution resulted in the change of its color to yellow then orange, and finally to dark orange indicating the formation of peroxo-titanium complexes. The solution was aged for additional 10 min during magnetic stirring, then the bottom inorganic phase was isolated by a separating funnel after 60 min of phase separation time. The sol was aged for 168 h at 40 °C then the temperature was raised for 48 h to 55 °C, since 40 °C was not sufficient to initiate the crystallization process when H_2O_2 was also added due to the high stability of peroxo-titanium complex [31]. In the latter step the temperature must be kept below 60 °C since above this temperature the formation of anatase occurred [32]. The suspension was dried at 40 °C then grounded in an agate mortar. As-prepared materials were washed 4 times by centrifugation using Milli-Q water. After the purification, the obtained powders were dried at 40 °C and ground again in an agate mortar prior to the photocatalytic experiments.

2.3. Characterization

A *Rigaku* diffractometer was used for the X-ray diffraction (XRD) measurements with the following parameters: $\lambda_{CuK\alpha}$ = 0.15406 nm, 40 kV, and 30 mA, 20–40° (2Θ) region. The average primary crystal size values were calculated using the Scherrer equation. The weight fraction of the rutile and anatase phases were estimated from the peak areas at 27.5 (2Θ) and 25.3 (2Θ), respectively.

A *Jasco-V650* spectrophotometer with an integration sphere (ILV-724) was used for measuring the DR (diffuse reflectance) spectra of the samples (λ = 220–800 nm). To obtain the band-gap energy the reflectance data were converted to F(A) values according to the Kubelka-Munk theory. The band gap was obtained from the plot of $[F(A)\,E]^{1/2}$ versus energy of the exciting light (E). The possible electron transitions were evaluated by plotting the dR/dλ vs. λ, where R is the reflectance and λ is the wavelength [33].

The specific surface areas of the catalysts were determined by N_2 adsorption at 77 K, using a BELCAT-A device. The specific surface area was calculated via the BET method.

The IR spectra were recorded by using a *Bruker Equinox 55* spectrometer. Samples were ground with KBr pressed into thin pellets (thickness ~0.3 mm) and the spectra were recorded with a spectral resolution of 2 cm^{-1}.

XPS measurements were performed on a *Specs Phoibos 150 MCD* system employing a monochromatic Al-K_α source (1486.6 eV) at 14 kV and 20 mA, a hemispherical analyser and charge neutralization device. Samples were fixed on a double-sided carbon tape and care was taken to ensure that the sample particles covered the tape. Experiments were performed by operating the X-ray source with a power of 200 W, while the pressure in the analyse chamber was in the range of 10^{-9}–10^{-10} mbar. The binding energy scale was charge referenced to the C1s at 284.6 eV. High resolution O1s and Ti2p spectra were obtained using analyzer pass energy of 20 eV in steps of 0.05 eV for analyzed samples. Analysis of the data was carried out with *Casa XPS* software.

2.4. Determination of photocatalytic performances

The photocatalytic activity was evaluated by phenol decomposition under visible light irradiation. The experiments were carried out in a double-walled glass vessel which was surrounded by four conventional energy saving compact fluorescence lamps (*Düwi 25920/R7S-24W*). The spectrum of the lamps was slightly modified by circulating 1 M sodium nitrite (*Molar Chemicals*, min. 99.13%) aqueous solution in the thermostating jacket (T = 25.0 °C). This $NaNO_2$ solution absorbs UV photons, therefore provides solely visible light irradiation for the suspension (Fig. S1). During the tests, air was bubbled through the reactor to provide a constant concentration of dissolved oxygen. For the experiments 0.1 mM phenol solution was used which contained the TiO_2 samples in 1.0 g L^{-1} concentration. Prior to the photocatalytic experiments the suspensions were sonicated in dark for 5 min, then it was vigorously stirred by a magnetic stirrer during the measurements. Changes

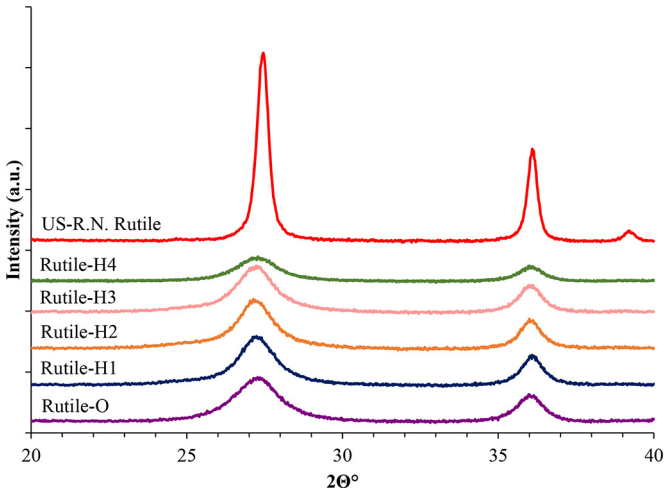

Fig. 1. X-ray diffraction patterns of the investigated rutile phase TiO_2-s.

in phenol concentration were measured by an *Agilent 1100* series HPLC system equipped with a *Lichrospher RP 18* column using methanol/water mixture (50:50) as eluent. Detection wavelength was set to be at the lower wavelength absorption maximum of phenol (λ = 210 nm). Reusability of the most active TiO_2 was examined by three consecutive phenol degradation measurements and between these experiments 24 h of UV irradiations were applied for the purification of the TiO_2 from the adsorbed oxidation by-products.

For some additional measurements the decomposition of Rhodamine B dye and the formation of hydroxyl radicals (via the formation of 7-hydroxycoumarin using fluorimetric detection) was investigated in case of Rutile-O and Rutile-H2 titania. The measurements were carried out in the same photoreactor as in which the phenol decomposition experiments were executed. The concentration of Rhodamine B (c_0 = 0.05 mM) was determined by an *Agilent 8453* spectrophotometer and the detection wavelength was λ = 553 nm using a 0.2 cm cuvette. The amount of formed OH• can be measured based on the formation of 7-hydroxycoumarin [34] (Eq. (1)). The fluorescence emission spectrum (excited at 332 nm, emission at 455 nm) of 7-hydroxycoumarin was measured by a *F-4500 HITACHI* fluorimeter in a 1 cm cuvette ($c_{0,coumarin}$ = 0.1 mM). Both the emission and excitation slits were set to 5.0 nm, the PMT voltage was 700 V during the measurements and the temperature of the solution was adjusted to 20 °C. The concentration of 7-hydroxycoumarin was determined by plotting the fluorescence intensity measured at 455 nm as a function of the concentration of the reference 7-hydroxycoumarin.

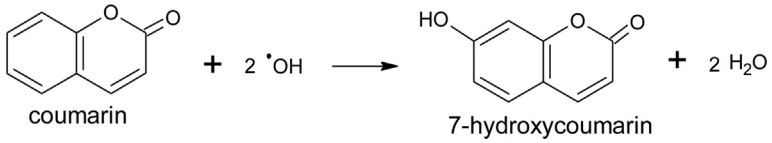

(1)

3. Results and discussion

3.1. Characterization of the photocatalysts

The crystal phases of the reference and various synthesized TiO_2-s were determined by X-ray diffraction (XRD) measurements (Fig. 1). The crystal phase distributions and the average primary particle sizes – estimated by the Scherrer equation – were presented in Table 1. The crystalline phase of the synthesized TiO_2-s were rutile (>99 wt%) and they had very small particle sizes (D = 5.2–7.3 nm). Aeroxide P25 contained 90 wt.% anatase and 10 wt% rutile ($D_{anatase}$ = 25.4 nm and D_{rutile} = 40 nm), while US-R.N. Rutile contained >99 wt% rutile (D = 30 nm). The specific surface areas of the self-made rutile titania varied within 178 and 285 $m^2\ g^{-1}$ (Table 1). Examining the results, it can be deduced, that applying hydrogen peroxide during the synthesis increased the specific surface area (from 178 $m^2\ g^{-1}$ to 237–285 $m^2\ g^{-1}$) compared to Rutile-O TiO_2.

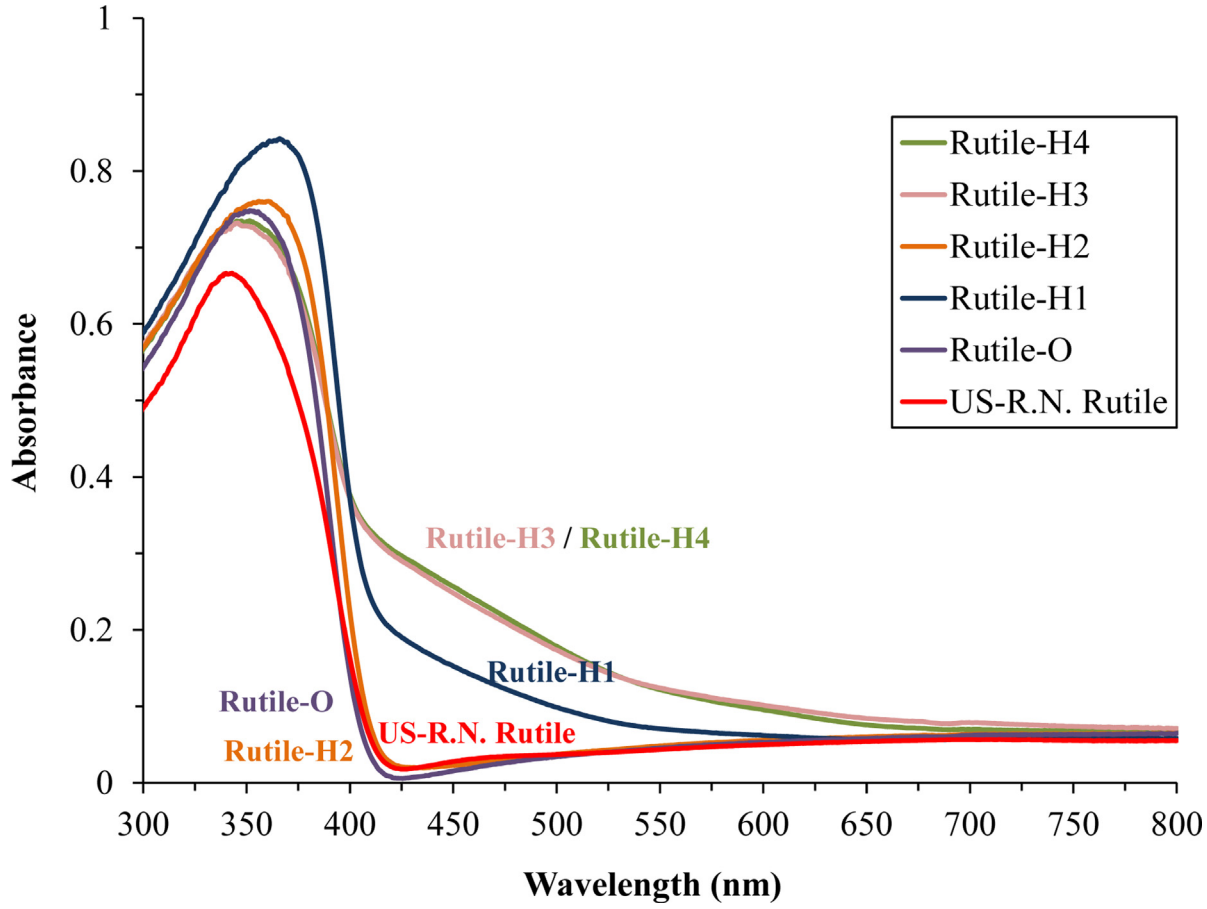

Fig. 2. DRS spectra of Rutile-O, Rutile-H1-Rutile-H4 and reference photocatalyst US-R.N. Rutile.

Table 1
Phase composition and the average primer particle sizes of the investigated TiO_2-s.

Titanium-dioxide	Phase composition				
	Anatase		Rutile		
	wt%	Particle size (nm)	wt%	Particle size (nm)	Specific surface area ($m^2\ g^{-1}$)
Rutile-O	–	–	>99	5.2	178
Rutile-H1	–	–	>99	7.3	285
Rutile-H2	–	–	>99	7	237
Rutile-H3	–	–	>99	6.8	246
Rutile-H4	–	–	>99	6.9	255
Aeroxide P25	90	25.4	10	40	49
US-R.N. Rutile	–	–	>99	30	46

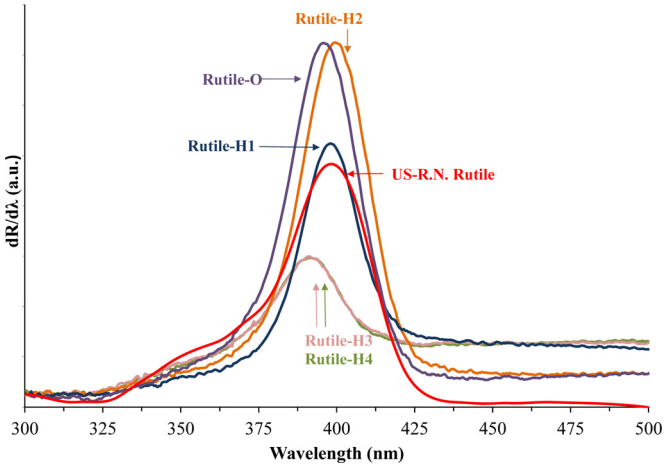

Fig. 3. First order derivative of the DRS spectra.

The light absorption of the TiO_2-s were determined by diffuse reflectance spectroscopy (DRS). As it can be seen in Fig. 2 the Rutile-H1, Rutile-H3 and Rutile-H4 samples possess greater light absorption in the visible light region compared to the Rutile-O, Rutile-H2 TiO_2-s. The band gap energies obtained by the Kubelka-Munk method were 3.07, 3.00, 3.05, 2.91, 2.92 and 3.02, 3.11 for Rutile-O, Rutile-H1-Rutile-H4 and reference photocatalysts US-R.N. Rutile and P25, respectively. Based on the results reported by Flak and his co-workers [33], by plotting the first-order derivatives of the DRS spectra as a function of wavelength, the dependence of the excitability from the wavelength can be determined more reliably. By applying such an approach we found that Rutile-H2 TiO_2 had the highest visible light absorption (visible light excitability) properties as it can be seen in Fig. 3.

Surface properties were characterized by IR spectroscopy. The IR spectra (Fig. 4) showed, that the self-made TiO_2-s had a broad band centered at 3400 cm^{-1}, with a sharp band at 1630 cm^{-1} which can be attributed to the stretching and bending vibrations of the surface OH groups [35,36]. Peaks at 1334 cm^{-1}, 1533 cm^{-1} and 2357 cm^{-1} represent bonds containing carbon [35,37,38], which can be attributed either to residual contamination from the TiO_2 precursor, or to the CO_2 adsorbed on the surface. In our TiO_2-s (Rutile-H1-H4), the IR absorption signal at 687 cm^{-1} corresponding to Ti—O—O stretching vibrations (representing peroxo groups) [25,27,38,39] did not appear (and its intensity did not change with the H_2O_2 amount), meaning that either these TiO_2-s did not have peroxo groups on the surface, or their quantity were below the threshold of detection of the IR spectrometer.

3.2. Evaluation of photocatalytic activity

The phenol decay curves were presented in Fig. 5. Rutile-O had comparable photocatalytic performance to P25 (17% of the phenol was degraded), however Rutile-H3 and Rutile-H4 TiO_2-s had negligible photocatalytic activity. Rutile-H2 self-made TiO_2 possessed by far the best photocatalytic efficiency compared to the other self-made TiO_2-s in the series (26% of the phenol was degraded after 4 h of irradiation), exceeding the photocatalytic activity of refer-

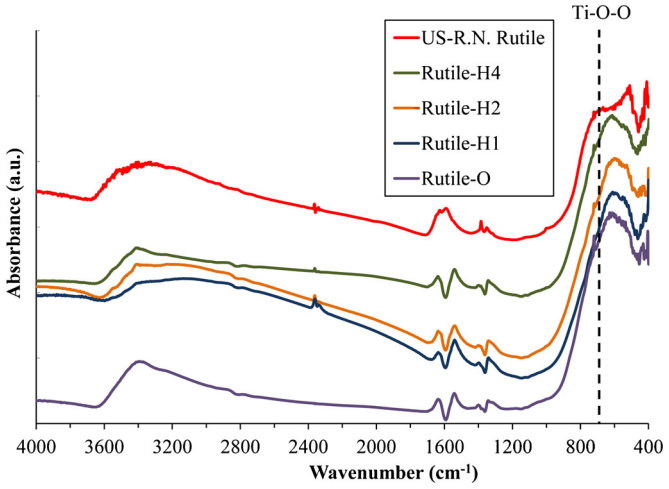

Fig. 4. IR spectra of the investigated TiO_2-s.

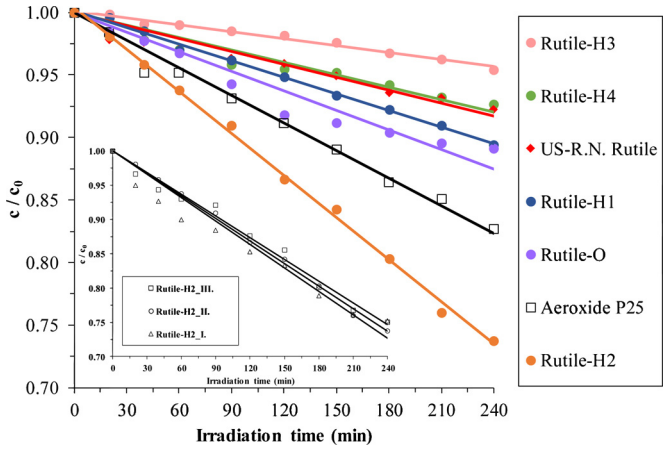

Fig. 5. Decay curves of phenol under VIS irradiation. The initial phenol concentration was set to 0.1 mM, and TiO_2 concentration was 1.0 g L^{-1}. Conventional 24 W energy saving compact fluorescence lamps with cut-off filtration were used (λ > 400 nm). The reusability of Rutile-H2 TiO_2 is represented in the inset.

ence photocatalysts Aeroxide P25 and US-R.N. Rutile as well. The reusability of Rutile-H2 TiO_2 was also determined by three consecutive phenol degradation measurements (the results are represented in the inset of Fig. 5). Results pointed out, that the photocatalyst had notable reusability, as it retained 98.4% of its initial photocatalytic efficiency after the measurements.

For some additional measurements Rutile-O (control titanium dioxide with no hydrogen peroxide used during the synthesis) and Rutile-H2 (the most efficient photocatalyst in case of phenol degradation) was selected to further establish the photocatalytic performance of these titania. The superior photocatalytic efficiency of Rutile-H2 compared to Rutile-O was observable in both cases (Rutile-H2 was more efficient in the degradation of Rhodamine B by ~40% and in the formation of $OH^{\bullet}$ by ~65%, respectively).

From these results, it can be assumed, that Rutile-H2 may have different properties compared to the other TiO_2-s. To investigate the cause of the prominent photocatalytic activity, the measurements concerning the characterization of the photocatalysts were re-evaluated. XRD measurements could explain it in various ways. It is well-known, that the coexistence of anatase and rutile phase via their synergic effect can lead to increased photocatalytic performance [40], however in this study pure rutile phase titanium dioxides were obtained. Another explanation could be that higher specific surface area generally leads to higher photocatalytic activity [30], but in the series Rutile-H2 TiO_2 had the second lowest value (apart from Rutile-O) and Rutile-H1, Rutile-H3, Rutile-H4 titania (with higher specific surface area) possessed lower photocatalytic activity. Therefore, the increase of photocatalytic activity in case of Rutile-H2 TiO_2 cannot be explained by its specific surface area.

The next investigated parameter was the band-gap values estimated from the DRS spectra. It is generally accepted, that band gaps in the visible light region in most cases correspond to visible light activity [41], however as it was already stated in Section 3.1, all of the self-made TiO_2-s had comparable band-gaps and all in the visible light region (2.91-3.05 eV = 406.5–426 nm nm). However, examining the first order derivatives of the DRS spectra (Fig. 4), important differences can be seen, namely that the visible light absorption in case of Rutile-H2 TiO_2 was red shifted which could be beneficial for the photocatalytic efficiency in case of visible light irradiation [42]. Examining the descending part of the spectra (from right to left) the order of light absorption was in good accordance with the resulted (decreasing) photocatalytic activities. Based on the results of the XRD and DRS measurements, it can be concluded, that the reason of the increased photocatalytic activity in case of Rutile-H2 must be a surface related feature, therefore IR measurements were performed. Unfortunately they did not show any significant bands which could be attributed to the increased photocatalytic performance (e.g. notably increased quantity of lattice defects or hydroxyl groups [43]), moreover, the presence of peroxo groups could not be observed. It was deduced, that either the investigated titania samples did not have peroxo groups on the surface, or their quantity was below the detection limit of the IR spectrometer. To ascertain the latter statement, the more sensible X-ray photoelectron spectroscopy (XPS) measurements were performed.

3.3. XPS measurements

As it was already stated in the section where the IR spectra were analyzed, no specific H_2O_2 related signals were detected, meaning that the sought species must be found at the photocatalyst surface in a relatively low concentration. To elucidate this aspect XPS spectra were recorded.

To identify H_2O_2 residues O1s spectra were analyzed (Fig. 6) in-detail for three samples. The main component (80–93 at.%, Table 2) of the three spectra was the lattice oxygen located at 530.0–530.2 eV [43]. The second component (6–8.2 at.%, Table 2) was the surface OH groups, denoted as OH_O and detected at 531.0–531.4 eV [43]. Surface OH groups can be responsible for the hydrophilic character of the photocatalyst, which was already correlated with the activity (higher surface OH concentration → increased hydrophylicity → increased photoactivity towards the degradation of phenol). However, in our case the change in the concentration of OH_O was not significant and thus cannot be directly responsible for the observed photocatalytic activity [43]. Adsorbed water (denoted as H_2O_O) was also noticed at 532.9 eV [44], which can be associated with the hydrophilic character of the sample, signalized before by the OH_O. The amount of H_2O fixed on the surface was found in the 1.4–2.7 at.% in oxygen associated concentration values. Nevertheless, a low-binding energy oxygen was noticed at 528.6 eV, which belongs to surface oxygen defects and usually appears together with Ti^{3+} (in our case this was also detected, but not shown) [45].

Table 2
The identified species' concentration in the investigated samples.

Species (at.%)	Samples		
	Rutile – O	Rutile – H2	Rutile – H3
Oxide_O	92.45	82.56	90.67
H_2O_O	1.42	1.53	2.65
OH_O	6.13	8.16	6.68
Low_O	–	2.51	–
Peroxo_O	–	5.24	–

The most important signal was identified at 532.0 eV, which was attributed to peroxo group originating from the H_2O_2. Named as oxygenated species, they were found in layered oxide electrodes applicable in lithium batteries [46].

The absence of the H_2O_2 during the synthesis procedure resulted clearly in the absence of the signal concerning the signal at 532.0 eV. It was interesting that in the sample Rutile-H3 no peroxo group signal was detected, although, the OH_O component's maximum values shifts from sample to sample (three components fit with the presence of peroxo group was also attempted in case of Rutile-H3, with the same FWHM, Gaussian peak shape). This interesting behavior was also observed in the case of DRS spectra, where the electron transition bands were shifted towards the visible light region in the case of Rutile-H2, while the mentioned bands were located in the near UV region (samples Rutile-O and Rutile-H3). Peroxo_O was fixed on the surface of Rutile-H2 in 5.24 at.% which means 3493 ppm in mass reported concentration (estimation based on atomic radii and weight, bulk density and an average of 7 nm diameter, sphere-like titania particles), a rather low number. Despite of this, Rutile-H2 was the most active sample in the visible light degradation of phenol (as well as in the degradation of Rhodamine B and formation of $OH^{\bullet}$ compared to Rutile-O). This means that the detected peroxo groups must be responsible for the enhanced photocatalytic activity.

The stability of the peroxo groups was also investigated. After the measurements, surprising results were obtained, as the catalyst preserved its activity after the applied re-usage period (26.2%, 24.9% and 24.7% of phenol was degraded after the first, second and third re-use, respectively). The difference observed in the data can be attributed as experimental error. This was followed by the XPS measurement of the re-used catalyst. As it can be observed in the O1s spectrum (Fig. 6), the main species' dominance was not changed (lattice oxygen – Oxide_O at 530.0–530.2 eV [43] and surface OH groups OH_O at 531.0–531.4 eV [43]) compared to catalyst before use. The first major difference was the absence of low binding energy oxygen (previously at 528.6 eV [45]), which was present in the original sample. This points out that locally the Ti^{3+} oxidized to Ti^{4+} (which was also observable in the Ti2p spectrum –

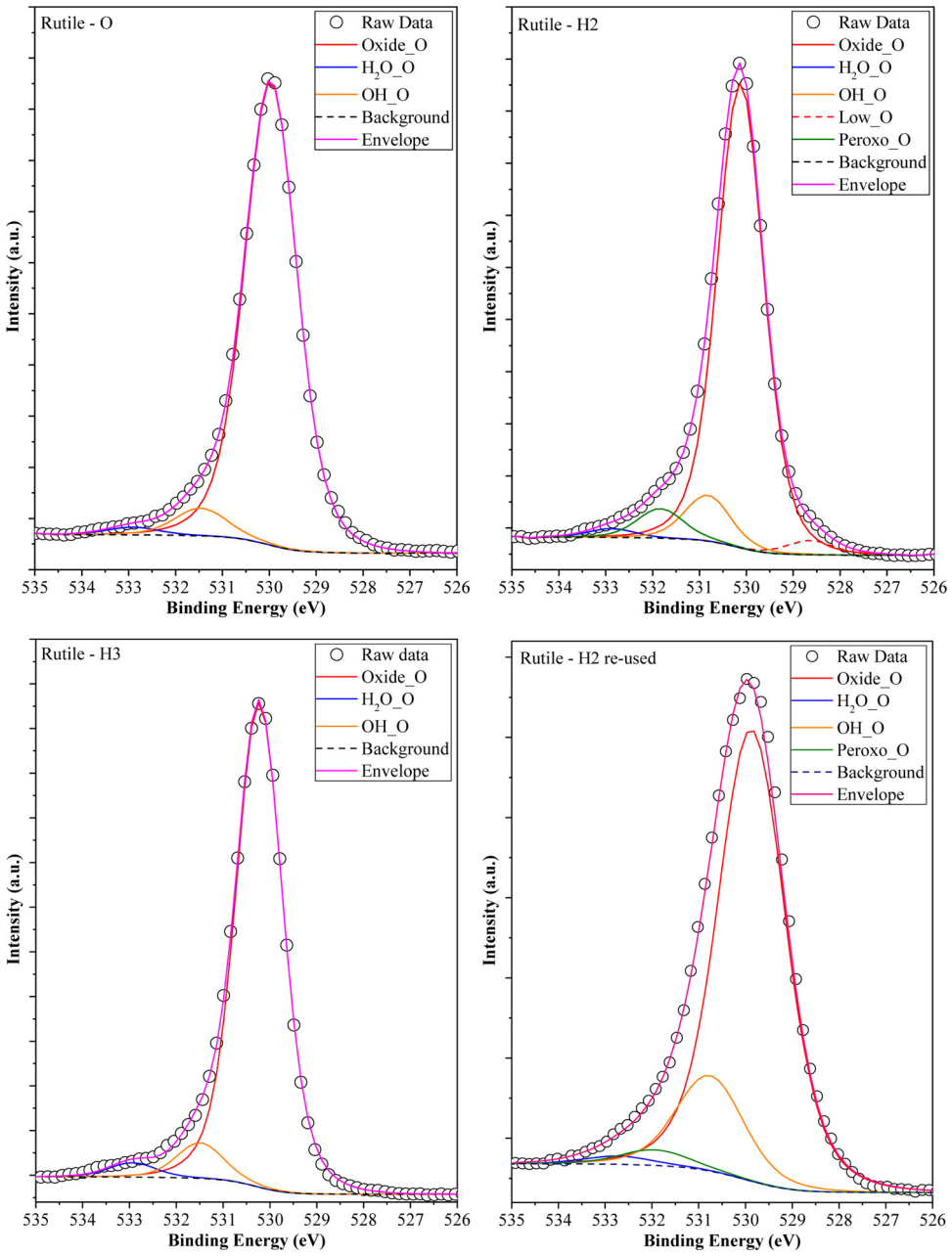

Fig. 6. High-resolution O1s XPS spectra of Rutile-O, Rutile-H2, Rutile-H3 samples and the three times re-used Rutile-H2, exposed to additional 72 h UV irradiation during the cleaning procedures.

not shown here), most probably due to the oxidation by the photo-generated holes [47]. Furthermore, it cannot be excluded that some of the amorphous matter crystallized at the surface of the catalyst, eliminating the previously mentioned Ti^{3+} which can be considered as crystal defects [47]. This change was accompanied by the slight increase of water related oxygen, which is logical, assuming that now the more fully coordinated Ti atoms can efficiently adsorb water [48]. Most importantly, the concentration of the peroxo groups was nearly halved after the experiment from 5.24 to 2.83 at.% from total oxygen. This show that these groups may possess a relative stability over medium time interval. Also it should be mentioned that the reusability experiment was carried out until total mineralization, exposing the catalyst to a further 24 h of UV light (3·24 h in total). However, the activity remained unchanged, because the existing recombination centers (Ti^{3+} – this specie is still considered with both positive and negative effects on the activity) disappeared, effect which presumably compensated the loss of the peroxo groups.

3.4. Why Rutile-H2?

It was very interesting that the mentioned peroxo groups were found only in the case of sample Rutile–H2. To get an answer concerning this matter, the knowledge available in the chemistry of titanium peroxo complexes should be applied. Peroxo complexes of titanium evolve from mononuclear to binuclear complexes depending on the pH.

In our case the pH slowly increased as the crystallization of titania occurred (at 55 °C). Moreover, the starting molar ratio of H_2O_2 and HCl differs, making possible several scenarios [31,49]:

- Starting point – hydrolysis (pH < 1): $Ti(H_2O)_6^{4+} + H_2O_2 \rightarrow TiO_2(H_2O)_4^{2+} + 2H^+ + 2H_2O$
- Deprotonation (pH = *1–3*): $TiO_2(H_2O)_4^{2+} \rightarrow TiO_2(OH)(H_2O)_3^{+} + H^+$
- Mono-bi nuclear transformation (pH > *3*): $2TiO_2(OH)(H_2O)_3^{+} \rightarrow Ti_2O_5(OH)^+ (H_2O)_6$

Considering the above-listed steps, in case of Rutile-H1 the amount of H^+ is too high, therefore no deprotonation is favored. Hence, when the polycondensation occurs (at higher pH values), the peroxo groups will not be included in the newly formed crystals. When the amount of H_2O_2 was too high (in the case of Rutile-H3 and Rutile-H4), all the above-mentioned steps occurred. However, the possibility of two neighboring Ti atoms being included in peroxo complexes is too high. Consequently, these entities will be unstable (multi peroxo compounds) and will be decomposed at 55 °C and eliminated from the system in the form of O_2. When the amount of H_2O_2 was optimal, the obtained surface peroxo groups were stable, as on the Ti atom only one peroxo complex bridge will be included with another Ti atom.

A plausible explanation for the increased photocatalytic efficiency caused by the peroxo groups could be following the steps listed below:

- The photogenerated electrons can roam freely the surface of the catalyst, and in some cases interparticular electron transfer can also occur
- When no specifically integrated compounds or surface groups are anchored the electron has no preferable localization site
- Peroxo groups, as they contain two oxygens can manifest their electron attracting inductive effect. By this, specific electron traps can be created, which can decrease the surface mobility of the electron.
- As the electrons are less mobile, their transfer to molecular oxygen is facilitated, resulting the well-known superoxide radical (which finally can yield •OH radicals [50]).

4. Conclusions

A series of nanosized rutile phase titanium dioxide samples was obtained by the addition of different amounts of hydrogen peroxide during the synthesis method. The optimal ratio of the added hydrogen peroxide was found to be $n_{Ti}:n_{H_2O_2} = 1:2$. Different ratios did not result in the appearance of peroxo groups in the series.

Photocatalytic activity measurements showed that Rutile-H2 had superior photocatalytic performance for phenol degradation under visible light irradiation compared to the other TiO_2-s in the series, exceeding the photocatalytic activity of reference photocatalysts (Aeroxide P25 and US-R.N. Rutile). The first order derivative of the DRS spectra pointed out that the order of light absorption of the investigated self-made TiO_2-s could be associated with the resulting photocatalytic performances, confirming the enhanced visible light excitability of sample Rutile-H2 caused by the peroxo groups.

IR measurements did not show peroxo groups in the self-made TiO_2-s presumably due to its lower limit of detection compared to XPS. XPS measurements, however, confirmed the formation of peroxo groups in our Rutile-H2 TiO_2.

Based on the literature, anchoring peroxo groups results in red shifted light absorption of UV active anatase phase TiO_2, however, to our best knowledge, forming peroxo groups on the surface of originally visible light active pure nanosized rutile have not been reported. In this study rutile phase TiO_2 containing peroxo groups was successfully synthesized at low temperature, and the optimal concentration of H_2O_2 was determined, which resulted in significantly higher visible light excitability.

Acknowledgements

The authors wish to express their deepest and sincerest recognition of Prof. András Dombi, a key figure in the topic of photocatalytic materials for the degradation of contaminants of environmental concern. Personal dedication of G.Veréb: "Dear András! You are the best supervisor ever! I am very thankful for all your professional support, and I am more grateful for our friendship! I say many thanks to you for everything!"

This project was supported by the János Bolyai Research Scholarship of the Hungarian Academy of Sciences. This research was partially co-financed by the Swiss Contribution (SH/7/2/20).

Appendix A. Supplementary data

Supplementary data associated with this article can be found, in the online version, at http://dx.doi.org/10.1016/j.cattod.2016.11.012.

References

[1] A. Fujishima, K. Honda, Nature 238 (1972) 37–38.
[2] J.-M. Herrmann, J. Matos, J. Disdier, C. Guillard, J. Laine, S. Malato, J. Blanco, Catal. Today 54 (1999) 255–265.
[3] M.G. Antoniou, D.D. Dionysiou, Catal.Today 124 (2007) 215–223.
[4] R. Kun, S. Tarján, A. Oszkó, T. Seemann, V. Zöllmer, M. Busse, I. Dékány, J. Solid State Chem. 182 (2009) 3076–3084.
[5] G. Veréb, Z. Ambrus, Z. Pap, Á. Kmetykó, A. Dombi, V. Danciu, A. Cheesman, K. Mogyorósi, Appl. Catal. A Gen. 417–418 (2012) 26–36.
[6] G. Veréb, L. Manczinger, G. Bozsó, A. Sienkiewicz, L. Forró, K. Mogyorósi, K. Hernádi, A. Dombi, Appl. Catal. B Environ. 129 (2013) 566–574.
[7] G. Veréb, L. Manczinger, A. Oszkó, A. Sienkiewicz, L. Forró, K. Mogyorósi, A. Dombi, K. Hernádi, Appl. Catal. B Environ. 129 (2013) 194–201.
[8] W. Bahnemann, M. Muneer, M.M. Haque, Catal. Today 124 (2007) 133–148.
[9] M. Qamar, B. Merzougui, D. Anjum, A.S. Hakeem, Z.H. Yamani, D. Bahnemann, Catal. Today 230 (2014) 158–165.
[10] K. Kovacs, J. Farkas, G. Vereb, E. Arany, G. Simon, K. Schrantz, A. Dombi, K. Hernadi, T. Alapi, J. Environ. Sci. Health B 51 (2016) 205–214.
[11] M. Gar Alalm, A. Tawfik, S. Ookawara, J. Environ. Chem. Eng. 4 (2016) 1929–1937.
[12] W. Lin, H. Zheng, P. Zhang, T. Xu, Appl. Catal. A Gen. 521 (2016) 75–82.
[13] A. Bonnefond, E. Gonzalez, J.M. Asua, J.R. Leiza, J. Kiwi, C. Pulgarin, S. Rtimi, Colloids Surf. B Biointerfaces 135 (2015) 1–7.
[14] S. Malato, P. Fernández-Ibáñez, M.I. Maldonado, J. Blanco, W. Gernjak, Catal. Today 147 (2009) 1–59.
[15] S. Malato, M.I. Maldonado, P. Fernández-Ibáñez, I. Oller, I. Polo, R. Sánchez-Moreno, Mater. Sci. Semicond. Process. 42 (2016) 15–23.
[16] E. Kowalska, Z. Wei, B. Karabiyik, A. Herissan, M. Janczarek, M. Endo, A. Markowska-Szczupak, H. Remita, B. Ohtani, Catal. Today 252 (2015) 136–142.
[17] C. Han, J. Andersen, V. Likodimos, P. Falaras, J. Linkugel, D.D. Dionysiou, Catal. Today 224 (2014) 132–139.
[18] E. Savinkina, L. Obolenskaya, G. Kuzmicheva, Appl. Nanosci. 5 (2014) 125–133.
[19] Y. Cho, W. Choi, C.-H. Lee, T. Hyeon, H.-I. Lee, Environ. Sci. Technol. 35 (2001) 966–970.
[20] É. Karácsonyi, L. Baia, A. Dombi, V. Danciu, K. Mogyorósi, L.C. Pop, G. Kovács, V. Coşoveanu, A. Vulpoi, S. Simon, Z. Pap, Catal. Today 208 (2013) 19–27.
[21] N.A. Ramos-Delgado, M.A. Gracia-Pinilla, L. Maya-Trevino, L. Hinojosa-Reyes, J.L. Guzman-Mar, A. Hernandez-Ramirez, J. Hazard. Mater. 263 (Pt 1) (2013) 36–44.
[22] K. Sahel, L. Elsellami, I. Mirali, F. Dappozze, M. Bouhent, C. Guillard, Appl. Catal. B Environ. 188 (2016) 106–112.
[23] G. Xiang, Y.G. Wang, D. Wu, T. Li, J. He, J. Li, X. Wang, Chemistry 18 (2012) 4759–4765.
[24] E.V. Savinkina, L.N. Obolenskaya, G.M. Kuzmicheva, E.N. Kabachkov, A.A. Gainanova, Y.V. Zubavichus, V.Y. Murzin, N.V. Sadovskaya, CrystEngComm 17 (2015) 7113–7123.
[25] J. Zou, J. Gao, F. Xie, J. Alloys Compd. 497 (2010) 420–427.
[26] L.-L. Tan, W.-J. Ong, S.-P. Chai, A.R. Mohamed, Chem. Eng. J. 283 (2016) 1254–1263.
[27] M.V. Shankar, T. Kako, D. Wang, J. Ye, J. Colloid Interface Sci. 331 (2009) 132–137.
[28] S. Yin, H. Hasegawa, D. Maeda, M. Ishitsuka, T. Sato, J. Photochem. Photobiol. A Chem. 163 (2004) 1–8.
[29] J. Noh, M. Yi, S. Hwang, K.M. Im, T. Yu, J. Kim, J. Ind. Eng. Chem. 33 (2016) 369–373.
[30] G. Veréb, T. Gyulavári, Z. Pap, L. Baia, K. Mogyorósi, A. Dombi, K. Hernádi, RSC Adv. 5 (2015) 66636–66643.
[31] J. Šubrt, P. Pulišová, J. Boháček, P. Bezdička, E. Pližingrová, L. Volfová, J. Kupčík, Mater. Res. Bull. 49 (2014) 405–412.

[32] Z.L. Tang, J.Y. Zhang, Z. Cheng, Z.T. Zhang, Mater. Chem. Phys. 77 (2003) 314–317.
[33] D. Flak, A. Braun, B.S. Mun, J.B. Park, M. Parlinska-Wojtan, T. Graule, M. Rekas, Phys. Chem. Chem. Phys. 15 (2013) 1417–1430.
[34] H. Czili, A. Horváth, Appl. Catal. B Environ. 81 (2008) 295–302.
[35] J. Orlikowski, B. Tryba, J. Ziebro, A.W. Morawski, J. Przepiórski, Catal. Commun. 24 (2012) 5–10.
[36] X. Ye, C. Zheng, L. Ma, X. Huang, Mater. Sci. Semicond. Process. 31 (2015) 295–301.
[37] C.G. Silva, J.L. Faria, Photochem. Photobiol. Sci. 8 (2009) 705–711.
[38] M.R. Ayers, A.J. Hunt, Mater. Lett. 34 (1998) 290–293.
[39] V. Etacheri, M.K. Seery, S.J. Hinder, S.C. Pillai, Adv. Funct. Mater. 21 (2011) 3744–3752.
[40] K.E. Rajashekhar, L.G. Devi, J. Mol. Catal. A Chem. 374–375 (2013) 12–21.
[41] Z. Pap, L. Baia, K. Mogyorósi, A. Dombi, A. Oszkó, V. Danciu, Catal. Commun. 17 (2012) 1–7.
[42] Á. Kmetykó, Á. Szániel, C. Tsakiroglou, A. Dombi, K. Hernádi, React. Kinet. Mech. Catal. 117 (2015) 379–390.
[43] Z. Pap, V. Danciu, Z. Cegléd, Á. Kukovecz, A. Oszkó, A. Dombi, K. Mogyorósi, Appl. Catal. B Environ. 101 (2011) 461–470.
[44] C.D. Wagner, D.A. Zatko, R.H. Raymond, Anal. Chem. 52 (1980) 1445–1451.
[45] Z. Pap, É. Karácsonyi, Z. Cegléd, A. Dombi, V. Danciu, I.C. Popescu, L. Baia, A. Oszkó, K. Mogyorósi, Appl. Catal. B Environ. 111–112 (2012) 595–604.
[46] D. Foix, M. Sathiya, E. McCalla, J.-M. Tarascon, D. Gonbeau, J. Phys. Chem. C 120 (2016) 862–874.
[47] L.-B. Xiong, J.-L. Li, B. Yang, Y. Yu, J. Nanomater. 2012 (2012) 1–13.
[48] S. Rtimi, J. Nesic, C. Pulgarin, R. Sanjines, M. Bensimon, J. Kiwi, Interface Focus 5 (2015) 20140046.
[49] J. Mühlebach, K. Müller, G. Schwarzenbach, Inorg. Chem. 9 (1970) 2381–2390.
[50] S. Ahmed, M.G. Rasul, W.N. Martens, R. Brown, M.A. Hashib, Desalination 261 (2010) 3–18.